J. Fluid Mech. (2010), *vol.* 642, *pp.* 349–372.
doi:10.1017/S0022112009991832

Stability of the flow of a Bingham fluid in a channel: eigenvalue sensitivity, minimal defects and scaling laws of transition

CHERIF NOUAR[1] AND ALESSANDRO BOTTARO[2]†

[1]LEMTA, UMR 7563 (CNRS-INPL-UHP), 2 Avenue de la Forêt de Haye, BP 160 54504 Vandoeuvre Lès Nancy, France

[2]DICAT, Facoltà di Ingegneria, Università di Genova, Via Montallegro 1, 16145 Genova, Italy

(Received 4 April 2009; revised 26 August 2009; accepted 27 August 2009; first published online 8 December 2009)

It has been recently shown that the flow of a Bingham fluid in a channel is always linearly stable (Nouar *et al.*, *J. Fluid Mech.*, vol. 577, 2007, p. 211). To identify possible paths of transition we revisit the problem for the case in which the idealized base flow is slightly perturbed. No attempt is made to reproduce or model the perturbations arising in experimental environments – which may be due to the improper alignment of the channel walls or to imperfect inflow conditions – rather a general formulation is given which yields the transfer function (the sensitivity) for each eigenmode of the spectrum to arbitrary defects in the base flow. It is first established that such a function, for the case of the most sensitive eigenmode, displays a very weak selectivity to variations in the spanwise wavenumber of the disturbance mode. This justifies a further look into the class of spanwise homogeneous modes. A variational procedure is set up to identify the base flow defect of minimal norm capable of optimally destabilizing an otherwise stable flow; it is found that very weak defects are indeed capable to excite exponentially amplified streamwise travelling waves. The associated variations in viscosity are situated mostly near the critical layer of the inviscid problem. Neutrally stable conditions are found as function of the Reynolds number and the Bingham number, providing scalings of critical values with the amplitude of the defect consistent with previous experimental and numerical studies. Finally, a structured pseudospectrum analysis is performed; it is argued that such a class of pseudospectra provides information well suited to hydrodynamic stability purposes.

Key words: instability, transition to turbulence, viscoelasticity

1. Introduction

Viscoplastic materials exhibit solid-like behaviour when the applied stress is 'low', and liquid-like behaviour at 'high' stresses. They are also called yield-stress materials since it is common in engineering applications to model them by introducing a yield stress τ_0, above which the material strains continuously, without recovery of strain upon removal of the applied stress. Below the threshold value τ_0 the material will not deform, however long the stress is maintained. The solid-like behaviour is associated

† Email addresses for correspondence: cherif.nouar@ensem.inpl-nancy.fr, alessandro.bottaro@unige.it

with elasticity, whereby the continuum deforms when subject to a given stress and there is complete strain recovery when the forcing is removed. In many cases, it is acceptable to neglect the elastic behaviour, by considering that the strain rate vanishes when the stress is below τ_0 (Coussot 1999). In this paper we follow this assumption, with all the caveats implicit in the physical concept of a yield stress (see the paper by Barnes 1999 for an exhaustive discussion of the debatable, but useful, concept of yield stress), and consider fluids without thixotropy, i.e. without time-dependent decrease of fluid viscosity under shear.

There are many classes of materials exhibiting a yield stress (Bird, Dai & Yarusso 1983), like slurries, pastes and suspensions, which contain a relatively high volume concentration of solid particles dispersed in a liquid. Examples include drilling muds in the oil industry, clays, cements, paints, printing inks, thickened hydrocarbon greases, certain asphalts and bitumens, cosmetical and pharmaceutical preparations, blood, plastic rocket propellant and a large variety of food products. The range of applications of viscoplastic materials, and their commercial relevance, is so large that it is essential to characterize these materials properly and understand their flow behaviour.

The Bingham model is used in this work to describe the continuum; the model is simple, but it contains all the ingredients of viscoplastic materials, namely a yield stress and a nonlinear variation of the effective viscosity. Two kinds of difficulties can be encountered when working with Bingham fluids (and even with more complex rheological models, such as the Casson, the Herschel–Bulkley or the Robertson–Stiff model). The first is that the yield stress of a given material is very difficult to define and measure in practice; usually rheometers are used either extrapolating shear stress–shear rate data to zero shear rate or by direct measurements of the creep/recovery type or with stress relaxation and stress growth techniques (cf. the review paper by Nguyen & Boger 1992). Other techniques exist, but the value of τ_0 provided is consistently just an estimate of the 'true' value. Part of the difficulty stems from the fact that typical laboratory viscometers do not work in the very low shear rate range, where data points deviate from the linear behaviour characteristic of larger strains; this is compounded by the realization that, when the applied stress slightly exceeds τ_0, the minimum time required for flow to be observed can be very large, to the point that the yield stress has been defined as 'a measurement of the experimenter's patience' (De Kee & Chan Man Fong 1993).

The second difficulty is that even when the yield stress is considered known, it is often not easy to determine the precise position of the yield surface (the interface between the sheared zone and the plug zone) since the problem is singular when the shear rate vanishes. Some form of smoothing of the effective viscosity of the Bingham model has been found necessary in several numerical applications (Bercovier & Engelman 1980; Lips & Denn 1984; Papanastasiou 1987; Beverly & Tanner 1992). A practical guidance on using different types of viscosity regularization and what one can expect by comparing with the exact model is provided in the paper by Frigaard & Nouar (2005).

Perhaps due to the factors above, the experimental and theoretical studies documenting the laminar–turbulent transition of yield-stress fluids in channels or ducts have produced contradictory and sometime confusing conclusions. Many early theories relied on the analysis of laboratory data, and led to empirical correlations for the onset of transition. Three configuration were investigated the most, the plane channel, the pipe and the concentric annulus, for their relevance to the chemical process industry (Hedström 1952; Metzner & Reed 1955; Dodge & Metzner 1959; Ryan & Johnson 1959; Shaver & Merrill 1959; Hanks & Christiansen 1962; Hanks

1963; Metzner & Park 1964; Meyer 1966; Hanks & Pratt 1967; Mishra & Tripathi 1971; Slatter 1999; Guzel, Frigaard & Martinez 2009*a*). The general approach relies on forming a parametric ratio of various flow quantities expected to affect the stability of the flow. For Newtonian fluids, the value of the parametric ratio at which the flow leaves the laminar regime is known or can be determined. The same value is then assumed to be valid for transition prediction in any purely viscous non-Newtonian fluid. However, when the rheological properties of the fluid depart significantly from Newtonian, the predictions provided by making such an assumption diverge (Nouar & Frigaard 2001), and there is no way to decide which criterion is preferable. It was observed that the critical Reynolds number determined using Hanks criterion (Hanks 1963) is the lowest one, with a behaviour like $B^{1/2}$ for large Bingham numbers B (the Bingham number is the non-dimensional ratio of yield stress to viscous stress). This scaling arises from the fact that the Bingham number effect was taken into account only through the width of the yielded region and the ensuing modification of the velocity gradient. Besides this, it was shown by Peixinho *et al.* (2005) and Esmael & Nouar (2008) for yield stress and shear-thinning fluids that transition occurs in two phases. At the end of the first phase, the mean flow profile is strongly deformed compared to that in the laminar regime. During the second phase there is a sharp increase of pressure drop, accompanied by the formation of turbulent spots. Clearly, using laminar flow solutions to generate transition criteria has severe shortcomings, although this has been done in several instances. Only a few papers (Abbas & Crowe 1987; Park *et al.* 1989; Escudier & Presti 1996; Escudier *et al.* 2005; Peixinho *et al.* 2005; Guzel *et al.* 2009*a*,*b*) have provided physical details of the transitional flow, through careful laser Doppler velocimetry (LDV) measurements of the axial and transverse velocity components. The latter three cited publications have highlighted the presence of low frequency oscillations near the pipe walls and asymmetric flow patterns close to the onset of transition; these observations are the most exciting fluid dynamical results so far, for the pipe flow case.

Among the geometrical configurations treated by Hanks & Pratt (1967) there was also the plane channel case; by defining a Reynolds and a Bingham number with the maximum fluid velocity, the density, the plastic viscosity, the yield stress and half the channel thickness, they reported an increase in transitional Reynolds number (Re from about 1.3×10^3 to about 2.9×10^4) with the increase of the Bingham number (B from about 0.5–300). On account of the fact that the viscosity of the Bingham fluid varies with the strain rate (whereas the plastic viscosity used in the dimensionless parameters above is constant), the transition correlation proposed in Hanks & Pratt (1967) has been much criticized, and several alternatives, based on the 'apparent' Newtonian viscosity evaluated at the wall and/or on the 'effective' hydraulic diameter, have been proposed. Although these debates have some importance, they cloud the real issue: a mechanistic explanation of transition is missing. In recent years, attention has thus turned to linear and nonlinear stability theories.

The first article on the linear stability of Bingham fluids in a plane channel is due to Frigaard, Howison & Sobey (1994). They focused on the asymptotic stability to two-dimensional travelling wave disturbances and found linearly increasing critical Reynolds numbers (Re_c) when the yield stress increased from zero. The complete formulation, equations and boundary conditions, was correctly given for the first time and it was shown in particular that the plug region remains unaffected by the disturbance field. However, the authors imposed even symmetry for the vertical velocity eigenfunction across the channel width, in analogy to the Newtonian case, and the results are consequently incomplete. Gupta (1999) made the same assumption for the channel flow linear stability of a general class of electrorheological fluids.

A few years later, Nouar & Frigaard (2001) carried out the first nonlinear stability analysis of a yield stress fluid, determining in particular the asymptotic behaviour of the energy Reynolds number Re_E (below which there is monotonic decay in time of the disturbance kinetic energy) in the limit of large B, finding that $Re_E = O(B^{1/2})$. The bounds imposed were not sharp because of the difficulties involved in dealing with dissipative terms. Such difficulties can be relaxed if the energy is calculated from the linear modal equations; this was the object of the paper by Frigaard & Nouar (2003), where it was reported that the most dangerous disturbance is a short wave with $Re_E = O(B^{3/4})$, for $B \to \infty$. Recently, Nouar *et al.* (2007) extended this energy bound to the case of small and moderate values of B and, perhaps more importantly, provided extensive modal and non-modal results on the growth of two- and three-dimensional perturbations. Computations were extended to very large values of Re and B, always without any hint of asymptotic instability. In hindsight this was justified by the analogy of this case with the Newtonian Couette–Poiseuille flow (Potter 1966), account being taken of the fact that the Bingham terms are always dissipative. The short-time stability analysis was conducted to verify whether non-modal disturbances were capable to extract much energy from the mean flow, at least transiently. The results by Nouar *et al.* (2007) reveal that in the small B limit the Newtonian Couette–Poiseuille case (characterized by optimal disturbances in the form of longitudinal vortices) is recovered (Bergström 2005); as B becomes of order one the most amplified initial disturbance becomes three dimensional. Significantly, smaller transient amplifications occur for increasing values of B, a trend consistent with experimental observations by Hanks & Pratt (1967).

The results given by Nouar *et al.* (2007) represent the premises on which the present contribution builds. Despite the importance of the transient growth mechanism, it is felt that knowledge of so-called optimal perturbations is still insufficient to explain the breakdown of the Bingham-fluid flow in a channel. This belief is corroborated by recent direct numerical simulations by Biau, Soueid & Bottaro (2008) for the flow of a Newtonian fluid in a duct of square cross-section, demonstrating that optimal disturbances fail to elicit a significant response from the flow in the nonlinear regime, whilst suboptimal disturbances can be very effective. Biau *et al.* (2008) report that transition is eventually triggered when the base flow of this otherwise linearly stable case is deformed sufficiently to withstand the exponential amplification of secondary disturbances.

In the present flow case the role of small base flow defects – and the ensuing viscosity variations – on the growth rate of instability modes is unknown. The issue is related to the non-normality and the pseudospectrum of the linear stability operator. The large transient growth that well-configured initial disturbances can express in this flow problem (Nouar *et al.* 2007) is already an effect of non-normality, and the relation between this concept and that of the ϵ-pseudospectrum has been clearly illustrated by Trefethen *et al.* (1993). Non-normality manifests itself through the extreme sensitivity of the stability operator to dynamical uncertainties of the system, which can be quantified by a disturbance operator (or matrix, in finite-dimensional space) Δ of norm ϵ. When all entries of the matrix Δ can be filled, we speak of 'unstructured perturbation analysis' and the conventional definition of the ϵ-pseudospectrum arises. On the other hand, it is perfectly conceivable that only a well-defined subset of the entries of the disturbance matrix Δ has non-zero terms, leading to a concept known as 'structured perturbation analysis' (Balas *et al.* 2001). The latter concept has not yet been exploited adequately in the stability analysis of fluid flows, while its use is becoming common in applications of optimal and robust control theory.

It will be shown here that minor base flow and viscosity differences with respect to the idealized model, positioned within the yielded region and optimally configured, are sufficient to cause exponential amplification of disturbances. This result brings up the receptivity issue: if small exogeneous disturbances, imperfect inlet conditions, or a slightly distorted base flow occur, the effect on the instability modes might be major. Whereas the ϵ-pseudospectrum lumps all these external effects under a unique definition, the ΔU-structured pseudospectrum (Bottaro, Corbett & Luchini 2003; Biau & Bottaro 2004) focuses on the effects of a single cause of deviation between the real and the ideal configurations.

The paper is organized as follows. Section 2 provides the equations and the base flow around which linearization is performed. Section 3 gives a detailed formulation of the disturbance equations for the general case of three-dimensional disturbances. In § 4 the sensitivity functions are obtained for structured operator's perturbations related to the presence of base flow and viscosity defects. Section 5 presents the formulation of the variational problem leading to the concept of minimal defects and discusses the results. In § 6 examples of ΔU-structured pseudospectra are given. Section 7 reports a parametric study of the neutral stability conditions by varying the norm of the defect and the yield stress; scaling laws are recovered and compared to literature results. Concluding remarks and perspectives are left for the last section.

2. Poiseuille flow of a Bingham fluid

We consider the flow of an incompressible Bingham fluid with a yield stress τ_0 and a plastic viscosity μ_p in a plane channel bounded by two solid walls in $y = \pm H^*$. The governing equations in dimensionless form are :

$$\nabla \cdot \boldsymbol{U} = 0, \tag{2.1}$$

$$\frac{\partial \boldsymbol{U}}{\partial t} + (\boldsymbol{U} \cdot \nabla)\, \boldsymbol{U} = -\nabla p + \nabla \cdot \boldsymbol{\tau}\,(\boldsymbol{U}), \tag{2.2}$$

where $\boldsymbol{U}$ is the velocity, p is the pressure and $\boldsymbol{\tau}$ is the deviatoric extra-stress tensor. The velocity vector is of the form $\boldsymbol{U} = U\boldsymbol{e}_x + V\boldsymbol{e}_y + W\boldsymbol{e}_z$, where U, V, W are the velocity components, and $\boldsymbol{e}_x$, $\boldsymbol{e}_y$, $\boldsymbol{e}_z$ are unit vectors in the streamwise x, normal to wall y and spanwise z directions, respectively. The above equations are rendered dimensionless using half the channel height H^* as length scale, the maximum velocity U_0^* of the basic flow as velocity scale, and ρU_0^{*2} to normalize stress and pressure. Using von Mises yield criterion, the dimensionless constitutive equations for Bingham fluids are

$$\boldsymbol{\tau} = \mu\, \dot{\boldsymbol{\gamma}} \quad \Leftrightarrow \quad \tau > \frac{B}{Re}, \tag{2.3}$$

$$\dot{\gamma} = 0 \quad \Leftrightarrow \quad \tau \leqslant \frac{B}{Re} \tag{2.4}$$

with

$$\mu = \frac{1}{Re}\left(1 + \frac{B}{\dot{\gamma}}\right). \tag{2.5}$$

Here $\dot{\gamma}$ and τ are respectively the second invariant of the strain rate $\dot{\boldsymbol{\gamma}}$ and of the deviatoric stress tensor $\boldsymbol{\tau}$ and μ is a dimensionless effective viscosity. The parameters B and Re are, respectively, the Bingham and Reynolds number, defined as

$$B = \frac{\tau_0\, H^*}{\mu_p\, U_0^*}, \quad Re = \frac{\rho\, U_0^*\, H^*}{\mu_p}. \tag{2.6}$$

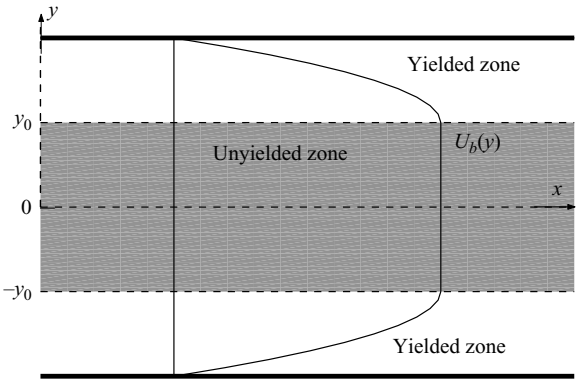

FIGURE 1. Poiseuille flow of Bingham fluid.

In the regions where the yield stress is not exceeded, the rate of strain tensor is identically zero and the stress tensor is undeterminate. The fluid within these unyielded (or plug) zones is constrained to move as a rigid body. The location of the yield surface is determined by enforcing $\tau = B/Re$, so that the motion of the yield surface is governed by the stress field in the yielded zone.

For one-dimensional shear flow, the expression of the axial velocity profile $U_b(y)$ is

$$U_b(y) = \begin{cases} 1, & 0 \leqslant |y| < y_0, \\ 1 - \left(\dfrac{|y| - y_0}{1 - y_0} \right)^2, & y_0 \leqslant |y| \leqslant 1, \end{cases} \tag{2.7}$$

sketched in figure 1. Using the relations : $|\tau_w| = B/(Re\, y_0)$ and $|\tau_w| = \frac{B}{Re}[1 + \frac{2}{B\,(1-y_0)}]$, where τ_w is the wall shear stress, it can be shown that the position y_0 of the yield surface is solution of the equation

$$B(1 - y_0)^2 - 2y_0 = 0. \tag{2.8}$$

For small and large B the following asymptotic relations for y_0 are easily found:

$$y_0 \sim \frac{B}{2} - \frac{B^2}{2} \qquad \text{as} \quad B \to 0\,, \tag{2.9}$$

$$y_0 \sim 1 - \sqrt{\frac{2}{B}} + \frac{1}{B} \quad \text{as} \quad B \to \infty. \tag{2.10}$$

It is clear that when $B \to 0$ the plug zone is reduced to the centreline, and the velocity profile approaches the Newtonian fluid profile. On the other hand, when $B \to \infty$ the plug zone fills almost the whole channel width, and the velocity profile is practically flat with a strong velocity gradient at the walls.

3. Linear stability approach

3.1. *Perturbation equations*

An infinitesimal perturbation $(\epsilon \boldsymbol{u}', \epsilon \mathrm{p}')$ (with $\epsilon \ll 1$) is imposed on the basic flow $(\boldsymbol{U}, P)$, so that the following equations are satisfied:

$$\boldsymbol{\nabla} \cdot [\boldsymbol{U} + \epsilon\, \boldsymbol{u}'] = 0, \tag{3.1}$$

$$\epsilon\, \boldsymbol{u}'_{\mathrm{t}} + [(\boldsymbol{U} + \epsilon\, \boldsymbol{u}') \cdot \boldsymbol{\nabla}][\boldsymbol{U} + \epsilon\, \boldsymbol{u}'] = -\boldsymbol{\nabla} \left(P + \epsilon p' \right) + \boldsymbol{\nabla} \cdot \boldsymbol{\tau}(\boldsymbol{U} + \epsilon\, \boldsymbol{u}'). \tag{3.2}$$

Wherever the yield stress is exceeded, the effective viscosity of the perturbed flow is expanded about the basic flow:

$$\mu\left(\boldsymbol{U}+\epsilon\boldsymbol{u}'\right)=\frac{1}{Re}\left[1+\frac{B}{|DU|}-\epsilon\left(\frac{\partial u'}{\partial y}+\frac{\partial v'}{\partial x}\right)\cdot\frac{B}{DU|DU|}+O\left(\epsilon^2\right)\right], \tag{3.3}$$

with $D\equiv \mathrm{d}/\mathrm{d}y$. Using (2.3) and (3.3), it is clear that $|\boldsymbol{\tau}(\boldsymbol{U}+\epsilon\boldsymbol{u}')-\boldsymbol{\tau}(\boldsymbol{U})|=\mathrm{O}(\epsilon)$. This means that the disturbance field can only linearly perturb the yield surface from its initial position:

$$y_y^{\pm}(\boldsymbol{U}+\epsilon\boldsymbol{u}')=\pm y_0\pm\epsilon h^{\pm}(x,z,t). \tag{3.4}$$

Disturbances are assumed to have the form

$$(u',v',w',p',h^{\pm})=[u(y,t),v(y,t),w(y,t),p(y,t),h^{\pm}(t)]\,\mathrm{e}^{\mathrm{i}(\alpha x+\beta z)}, \tag{3.5}$$

where α and β are the wavenumbers in the streamwise and spanwise directions. After some algebra (for details see Frigaard *et al.* 1994 and Nouar *et al.* 2007) it is obtained:

$$\mathrm{i}[\alpha u+\beta w]+Dv=0, \tag{3.6}$$

$$u_t=-\mathrm{i}\,\alpha\,U\,u-vDU-\mathrm{i}\alpha p+\frac{1}{Re}\mathscr{F}u+\frac{B}{Re}\left[\frac{-(\alpha^2+\beta^2)u-\mathrm{i}\alpha Dv}{|DU|}\right], \tag{3.7}$$

$$v_t=-\mathrm{i}\,\alpha\,U\,v-Dp+\frac{1}{Re}\mathscr{F}v+\frac{B}{Re}\left[D\left(\frac{2\,D\,v}{|DU|}\right)+\frac{-\beta^2\,v+\mathrm{i}\beta D\,w}{|DU|}\right], \tag{3.8}$$

$$w_t=-\mathrm{i}\,\alpha\,U\,w-\mathrm{i}\beta p+\frac{1}{Re}\mathscr{F}w+\frac{B}{Re}\left[D\left(\frac{\mathrm{i}\beta v+D\,w}{|DU|}\right)-\frac{(\alpha^2+\beta^2)\,w+\mathrm{i}\beta D\,v}{|DU|}\right] \tag{3.9}$$

with $\mathscr{F}\equiv D^2-k^2, k^2=\alpha^2+\beta^2$. The boundary conditions at the wall $y=1$ and at the interface $y=y_0$ are

$$u(1)=v(1)=w(1)=0, \tag{3.10}$$

$$u(y_0)=v(y_0)=w(y_0)=0, \tag{3.11}$$

$$Dv(y_0)=Dw(y_0)=0,\quad Du(y_0)=-h^{+}D^2U(y_0). \tag{3.12}$$

The system of equations (3.6)–(3.9) can be expressed in terms of u and v if $\alpha\neq 0$, or in terms of v and w if $\beta\neq 0$ (Nouar *et al.* 2007).

The case $\alpha=0$ can be dealt with by inspection observing that all modes are purely imaginary and always damped, for whatever base flow U. This fact, pointed out by Nouar *et al.* (2007), implies that whatever variation $\Delta U(y)$ in base flow is unable to trigger an instability in the form of longitudinal vortices. As a consequence the ΔU-structured pseudospectrum will never protrude into the unstable half-plane, unlike the unstructured pseudospectrum. The difference is due to the fact that the unstructured pseudospectrum allows a two-way coupling between the u and v equations, whereas it is easy to see that in the original system the u equation is forced by the vertical velocity v, whereas the v equation is homogeneous.

The (v,w) formulation of the problem, needed to treat the stability of streamwise-travelling modes and three-dimensional modes, reads

$$-\mathrm{i}\begin{pmatrix}\mathscr{L}_1 & \mathscr{L}_2\\ \mathscr{L}_3 & \mathscr{L}_4\end{pmatrix}\begin{pmatrix}v\\ w\end{pmatrix}=\frac{\partial}{\partial t}\begin{pmatrix}-\mathrm{i}Re\left(D^2-\alpha^2\right) & \beta\,Re\,D\\ -\mathrm{i}\beta\,Re\,D & Re\,k^2\end{pmatrix}\begin{pmatrix}v\\ w\end{pmatrix} \tag{3.13}$$

and, in space state form, common in control theory, communication and signal processing, it can be written as

$$\frac{\partial \boldsymbol{q}}{\partial t} = -\mathrm{i}\boldsymbol{M}^{-1}\boldsymbol{L}\boldsymbol{q}, \tag{3.14}$$

with $\boldsymbol{q} = (v, w)^T$ the vector of state variables. The elements of the matrix $\boldsymbol{L}$ are

$$\mathscr{L}_1 = \mathscr{F}^2 + \beta^2\mathscr{F} - \mathrm{i}\alpha ReU(D^2 - \alpha^2) + \mathrm{i}\alpha Re(D^2U) + \tag{3.15}$$

$$B\left[\frac{\alpha^2\beta^2}{|DU|} - (4\alpha^2 + \beta^2)\,D\left(\frac{D}{|DU|}\right)\right], \tag{3.16}$$

$$\mathscr{L}_2 = \mathrm{i}\beta\, D\mathscr{F} + \alpha\beta Re\,(UD + DU) - \mathrm{i}\beta B\left[k^2\,D\left(\frac{1}{|DU|}\right) + \frac{(k^2+\alpha^2)D}{|DU|}\right], \tag{3.17}$$

$$\mathscr{L}_3 = \beta\, D\mathscr{F} - \mathrm{i}\alpha\,\beta\, Re\,(U\,D - DU) - B\,\beta\left[\frac{(k^2+\alpha^2)\;D}{|DU|} + \alpha^2 D\left(\frac{1}{|DU|}\right)\right], \tag{3.18}$$

$$\mathscr{L}_4 = \mathrm{i}k^2\mathscr{F} + \alpha ReUk^2 + \mathrm{i}\,B\left[\frac{\alpha^2\,D^2 - k^4}{|DU|} + \alpha^2\,D\left(\frac{1}{|DU|}\right)\,D\right]. \tag{3.19}$$

The boundary conditions are $v = Dv = w = 0$ at the wall and at the yield surface.

3.2. *Eigenvalue problem*

Assuming solutions of the form $\boldsymbol{q} = \tilde{\boldsymbol{q}}\exp(-\mathrm{i}\,\omega t)$, where ω is the complex frequency, the initial value problem (3.14) is transformed into the following generalized eigenproblem for ω:

$$\boldsymbol{M}^{-1}\boldsymbol{L}\,(\tilde{v}, \tilde{w})^T = \omega\,(\tilde{v}, \tilde{w})^T\,. \tag{3.20}$$

The amplification of a given mode is given by ω_i, the imaginary part of the eigenvalue ω. The ratio $\omega_r/(\alpha^2 + \beta^2)^{0.5}$, with ω_r the real part of ω, corresponds to the phase speed of the wave travelling in the direction $(\alpha, 0, \beta)$.

3.3. *Domain mapping*

Since the width $(1 - y_0)$ of the yielded zone varies with B, it is useful to map the domain $[y_0, 1]$ into $[0, 1]$, by introducing the following reduced parameters:

$$x = \tilde{x}(1 - y_0), \quad y = \tilde{y}(1 - y_0) + y_0, \quad z = \tilde{z}(1 - y_0), \tag{3.21}$$

$$\tilde{\alpha} = \alpha\,(1 - y_0)\,, \quad \tilde{\beta} = \beta\,(1 - y_0)\,, \quad \tilde{\omega} = \omega\,(1 - y_0)\,, \tag{3.22}$$

$$\tilde{Re} = Re\,(1 - y_0)\,, \quad \tilde{B} = B\,(1 - y_0)\,. \tag{3.23}$$

Of course $\tilde{k}^2 = \tilde{\alpha}^2 + \tilde{\beta}^2$, $\tilde{D} \equiv \mathrm{d}/\mathrm{d}\tilde{y}$ and $\tilde{\mathscr{F}}^2 \equiv \tilde{D}^2 - \tilde{k}^2$. The use of $(\tilde{\cdot})$ variables does not modify the expressions of the initial value problem (3.14) nor the ensuing eigenproblem (3.20), but the base flow now reads

$$U = 1 - \tilde{y}^2 \qquad \text{for} \qquad \tilde{y} \in [0, 1]\,. \tag{3.24}$$

In the following, the $(\tilde{\cdot})$ notation will be dropped with no ambiguity, lest it to be remarked that from now on Re, B and α are scaled with a length scale which characterizes the shear zone, except in figure 11 where unscaled parameters are represented as also indicated in the caption.

4. Sensitivity functions for structured operator's perturbations

It has recently been shown by Nouar *et al.* (2007) that the matrix $\boldsymbol{M}^{-1}\boldsymbol{L}$ is highly non-normal, reflecting a strong sensitivity of the normal modes to operators' perturbations.

Here we focus on a structured set of such perturbations, assuming infinitesimal variations in the base flow profile δU. These variations cause corresponding variations in the eigenvalues and eigenfunctions of the operator $\boldsymbol{M}^{-1}\boldsymbol{L}$:

$$U \to U + \delta U \Rightarrow \begin{cases} \omega \to \omega + \delta\omega, \\ v \to v + \delta v, \\ w \to w + \delta w. \end{cases} \tag{4.1}$$

Introducing (4.1) into (3.20) it is found

$$\delta\boldsymbol{M}^{-1}\boldsymbol{L}\,\boldsymbol{q} + \boldsymbol{M}^{-1}\delta\boldsymbol{L}\boldsymbol{q} + \boldsymbol{M}^{-1}\,\boldsymbol{L}\delta\boldsymbol{q} = \delta\omega\boldsymbol{q} + \omega\delta\boldsymbol{q}, \tag{4.2}$$

with $\delta\boldsymbol{L} = (\partial\boldsymbol{L}/\ \partial U)\delta U$, $\delta\boldsymbol{M}^{-1}$ the zero matrix, and $\delta\boldsymbol{q} = (\delta v, \delta w)^T$. We now project (4.2) onto the adjoint subspace, with the eigenvector $\boldsymbol{a}(y) = (a, b)^T$ solution of the adjoint problem $\boldsymbol{M}^{+-1}\boldsymbol{L}^{+}\boldsymbol{a} = \omega\boldsymbol{a}$, to find the resulting eigenvalue variation:

$$\delta\omega = \frac{(\boldsymbol{a}, \boldsymbol{M}^{-1}\delta\boldsymbol{L}\boldsymbol{q})}{(\boldsymbol{a}, \boldsymbol{q})} = (\mathscr{G}_U, \delta U). \tag{4.3}$$

The sensitivity function $\mathscr{G}_U$ quantifies the effect of an infinitesimal modification of the base flow δU on a given eigenvalue ω. The expression of the sensitivity functions for three-dimensional modes is

$$\mathscr{G}_U = \frac{\mathscr{I}_1 + B\,\mathscr{I}_2}{\int_0^1 \mathscr{I}_3\,\mathrm{d}y} \tag{4.4}$$

with $\mathscr{I}_1$, $\mathscr{I}_2$ and $\mathscr{I}_3$ given in the Appendix. The adjoint variables introduced above rely on the following definition of inner product: $(f, g) \equiv \int_0^1 f\,g\,\mathrm{d}y$, and the matrices $\boldsymbol{L}^+$ and $\boldsymbol{M}^+$ of the adjoint eigenproblem are

$$\boldsymbol{L}^+ \equiv \begin{pmatrix} \mathscr{L}_1^+ & \mathscr{L}_2^+ \\ \mathscr{L}_3^+ & \mathscr{L}_4^+ \end{pmatrix} \tag{4.5}$$

and

$$\boldsymbol{M}^+ \equiv \begin{pmatrix} -\mathrm{i}Re\,(D^2 - \alpha^2) & \mathrm{i}\beta\,Re\,D \\ -\beta\,Re\,D & Re\,k^2 \end{pmatrix} \tag{4.6}$$

with

$$\mathscr{L}_1^+ = \mathscr{F}^2 + \beta^2\,\mathscr{F} - \mathrm{i}\alpha\,Re\,U\,(D^2 - \alpha^2) - 2\,\mathrm{i}\alpha\,Re\,DU\,D + \tag{4.7}$$

$$B\left[\frac{\alpha^2\,\beta^2}{|DU|} - (4\alpha^2 + \beta^2)\ D\left(\frac{D}{|DU|}\right)\right] \tag{4.8}$$

$$\mathscr{L}_2^+ = -\beta\,D\,\mathscr{F} + \mathrm{i}\alpha\,\beta\,Re\,[U\,D + 2\,DU] + \tag{4.9}$$

$$\beta\,B\,\left[(k^2 + \alpha^2)\,\frac{D}{|DU|} + k^2\,D\left(\frac{1}{|DU|}\right)\right] \tag{4.10}$$

$$\mathscr{L}_3^+ = -\mathrm{i}\beta\,D\mathscr{F} - \alpha\,\beta\,Re\,U\,D + \mathrm{i}\beta\,B\left[\alpha^2\,D\left(\frac{1}{|DU|}\right) + \frac{k^2 + \alpha^2}{|DU|}D\right] \tag{4.11}$$

$$\mathscr{L}_4^+ = \mathrm{i}\,k^2\,\mathscr{F} + \alpha\,Re\,U\,k^2 + \mathrm{i}B\left[\frac{\alpha^2\,D^2 - k^4}{|DU|} + \alpha^2\,D\left(\frac{1}{|DU|}\right)\ D\right]. \tag{4.12}$$

The two-dimensional $\beta = 0$ case appears to be very relevant on account of a theorem demonstrated by Georgievskii (1993) for viscoplastic fluids which holds that 'among

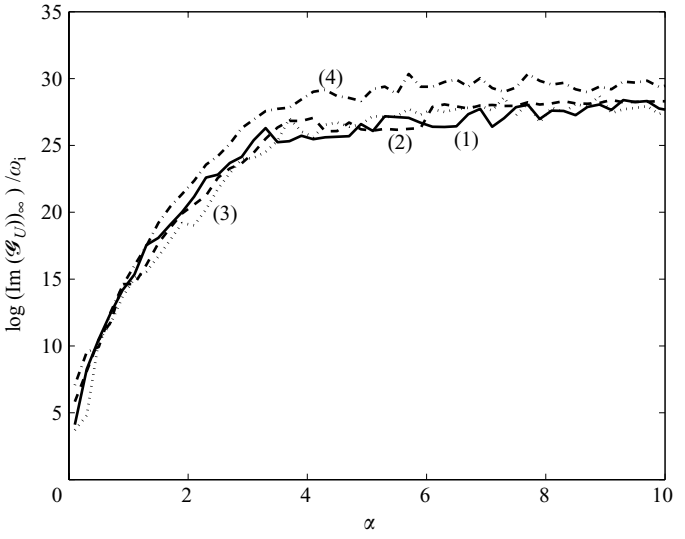

FIGURE 2. Logarithm of the infinity norm of $[\mathrm{Im}(\mathscr{G}_U)]/\omega_i$ of the most sensitive mode versus α at $Re = 5 \times 10^3$. The continuous line (1) and the dashed line (2) correspond to the Newtonian Couette–Poiseuille situation, i.e. $B = 0$, and, respectively, $\beta = 0$ and $\beta = 8$. The dotted curve (3) and the dashed-dotted curve (4) correspond to the Bingham–Poiseuille flow with $B = 18$ and, respectively, $\beta = 0$ and $\beta = 8$.

all amplified three-dimensional disturbances that satisfy the condition $\dot{\gamma}_{yz} = 0$ we can always find a two-dimensional disturbance (in the plane of the basic motion) that grows at the same rate, for the same value of B and smaller Re number'. Although the condition on $\dot{\gamma}_{yz} = \mathrm{i}\beta v + Dw$ is sufficient to guarantee the validity of this Squire-like theorem, it greatly narrows the class of perturbations under consideration. It seems thus appropriate to assess right away the sensitivity of two- and three-dimensional disturbances to variations in the base flows, to decide whether a particular class of disturbances appears to be preferentially selected by environmental conditions.

From (4.3), assuming that δU is a properly normalized Dirac distribution centred on the position where the modulus of $\mathrm{Im}(\mathscr{G}_U)$ is maximum, it is easy to see that the relative displacement (along the imaginary axis) of each eigenmode from its reference position is proportional to $\max[\mathrm{Im}(\mathscr{G}_U)]/\omega_i$. In such a function, the large value of the ∞-norm of $\mathrm{Im}(\mathscr{G}_U)$ for large α is compensated by the large absolute value of the growth rate of the corresponding stable mode. We have thus plotted this quantity against α in figure 2, for the most sensitive eigenmode, for two values of β and two Bingham numbers, $B = 0$ and $B = 18$ (this latter value corresponds to a base flow in which the unyielded zone of figure 1 occupies 90 % of the available space). The results show that at $B = 0$ (which corresponds to the Newtonian Couette–Poiseuille flow) there is a mild variation of the sensitivity with the spanwise wavenumber β; the sensitivity grows until a value of α approximately equal to 4, and then its value saturates. The lack of smoothness of the lines is related to the less-than-perfect identification of the eigenvalues for large αs, particulary at the intersection of the A, P and S branches. The behaviour is similar for the larger B case, although now there is a slightly larger difference in the sensitivity between the two values of β plotted. Despite this, it seems fair to state that the effect of β is secondary and the statement is confirmed by many more cases (not shown) tested for varying B and β. We thus

decided to limit the investigation to the simpler situation of z-independent instability modes.

4.1. *Spanwise homogeneous disturbances, $\beta = 0$*

For the case of spanwise homogeneous disturbances the matrices $\boldsymbol{L}$ and $\boldsymbol{M}$ are diagonal, and the normal v and longitudinal w components of the velocity are decoupled, and likewise for their adjoints. Furthermore, the eigenproblem for w is Hermitian, and its spectrum is formed by modes which are always stable, so that in the sensitivity problem only v modes are important. The v eigenproblem is described by an Orr–Sommerfeld-like equation

$$\mathscr{L}_{os} v = -\mathrm{i}\,\omega\, Re\,(D^2 - \alpha^2)v, \tag{4.13}$$

where

$$\mathscr{L}_{os} = (D^2 - \alpha^2)^2 - \mathrm{i}\alpha\, ReU(D^2 - \alpha^2) + \mathrm{i}\alpha\, Re\, D^2 U + B\left[-4\alpha^2 D\left(\frac{D}{|DU|}\right)\right] \tag{4.14}$$

with boundary conditions

$$y = 0; \quad v = Dv = 0; \tag{4.15}$$

$$y = 1; \quad v = Dv = 0. \tag{4.16}$$

The additional condition $D^2 v(0) = \mathrm{i}\alpha h^+ D^2 U(0)$ can be used to recover the amplitude of the yield surface deformation. The adjoint eigenvalue problem is

$$\mathscr{L}^+_{os} a = -\mathrm{i}\,\omega\, Re\ (D^2 - \alpha^2)a \tag{4.17}$$

with

$$\mathscr{L}^+_{os} \equiv (D^2 - \alpha^2)^2 - \mathrm{i}\alpha\, ReU(D^2 - \alpha^2) - 2\mathrm{i}\alpha\, ReDU\,D + B\left[-4\alpha^2 D\left(\frac{D}{|DU|}\right)\right], \tag{4.18}$$

and same boundary conditions as for the direct equation. The terms proportional to B in (4.14) and (4.18) are the same, indicating that non-normality of $\mathscr{L}_{os}$ arises uniquely from the inertial terms, like in the Newtonian case.

An example of the eigenvalues spectrum for $\alpha = 1$, $Re = 5000$ and $B = 2$ is shown in the left frame of figure 3 and, in analogy to the Newtonian case (Mack 1976), the branches have been labelled as 'A', 'P' and 'S'. We have verified that the spectrum is identical for the direct and the adjoint problems. The effect of the yield stress is to produce a misalignment of wall modes (branch A) and yield surface modes (branch P). For each mode, the sensitivity function is defined by

$$\mathscr{G}_U = \frac{\mathrm{i}\alpha\,(\alpha^2 a v + v D^2 a + 2Da\,Dv) + \mathrm{sign}(DU)\left(\dfrac{B}{Re}\right)\left[(4\alpha^2)D\left(\dfrac{Da\,Dv}{(DU)^2}\right)\right]}{\int_0^1 \mathrm{i}(\alpha^2 a v + Da\,Dv)\mathrm{d}y,} \tag{4.19}$$

where the parameter $\mathrm{sign}(DU)$ is $+1$ for positive DU, -1 otherwise. In the Newtonian limit the expression of $\mathscr{G}_U$ of (4.19) coincides with that given by Bottaro *et al.* (2003). The yield stress introduces a shear thinning behaviour which appears in the function $\mathscr{G}_U$ through the term proportional to B/Re; this term is not singular when $DU \to 0$ (as a simple application of l'Hôpital rule can show), although it could cause numerical difficulties. The right frame of figure 3 displays the infinity norm of $\mathscr{G}_U$ for the first 30 eigenvalues: modes near the crossing of branches, labelled with the numbers 12, 13 and 14 in the left frame of the figure, display the largest norm, coherently with

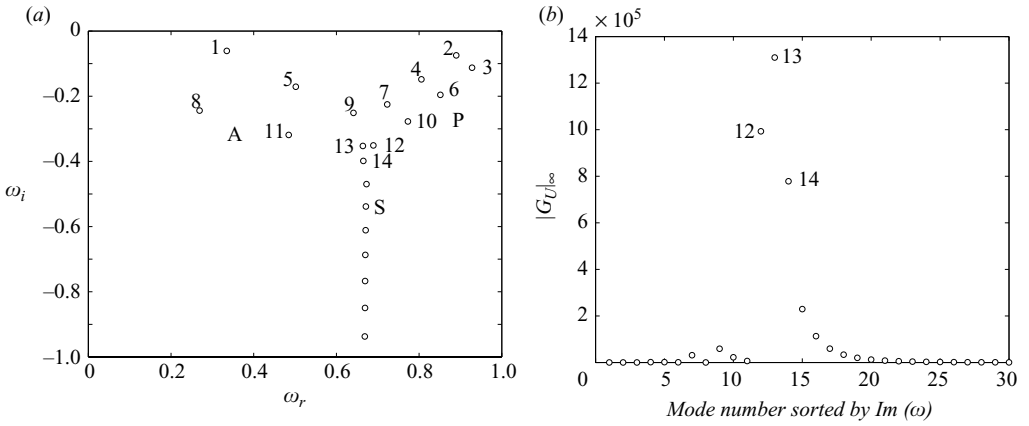

FIGURE 3. (*a*) Eigenvalue spectra at $Re = 5 \times 10^3$, $B = 2$ and $\alpha = 1$. (*b*) Infinity norm of the first 30 sensitivity functions, sorted by the imaginary part of ω.

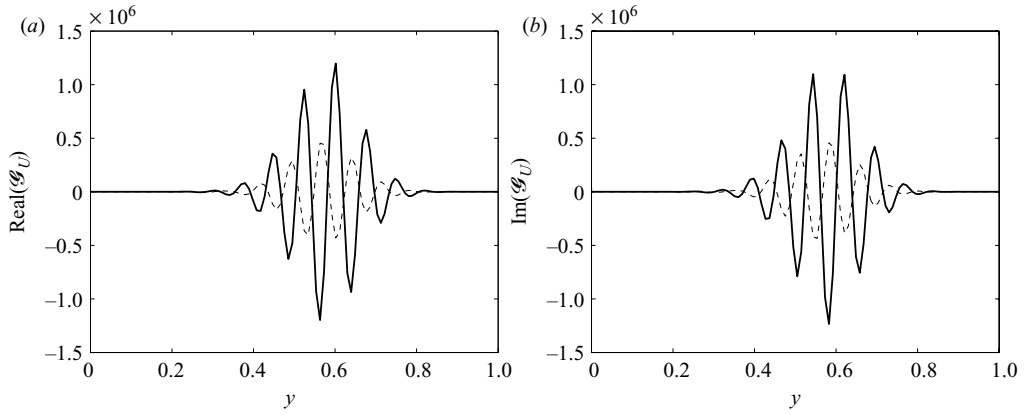

FIGURE 4. Real part (*a*) and imaginary part (*b*) of $\mathscr{G}_U$ for the most sensitive eigenvalues at $B = 2$ (continuous line) and $B = 20$ (dashed line), at $Re = 5000$ and $\alpha = 1$.

ϵ-pseudospectra drawn by Nouar *et al.* (2007). Mode 13 responds the most to an infinitesimal deformation of the base flow, whereas all the near-wall modes (1, 5, 8 and 11) displays very weak sensitivity to variations in U. These trends (and the order of magnitude of the sensitivity functions) are consistent with those that we have found for the case of the Couette–Poiseuille flow of a Newtonian fluid.

In figure 4 the real and imaginary parts of the sensitivity function for the most sensitive modes at two values of the Bingham number, $B = 2$ and $B = 20$, are shown. The eigen-spectra are very similar with varying B, and so are the plots of real and imaginary parts of $\mathscr{G}_U$. The base flow variations which affects growth rate and frequency the most are localized near the centre of the yielded region, with a support of about half a unit of length. The ∞ norm of the most sensitive eigenmode remains always of the same order as that of the Couette–Poiseuille flow of a Newtonian fluid ($B = 0$) as it is shown in figure 5, where the ratio between the maximum value of $|\mathscr{G}_U|_\infty$ and the maximum value of $|\mathscr{G}_U|_\infty$ when $B = 0$ is drawn as function of B for different Re. One can note that the dependency on Re is not monotonic.

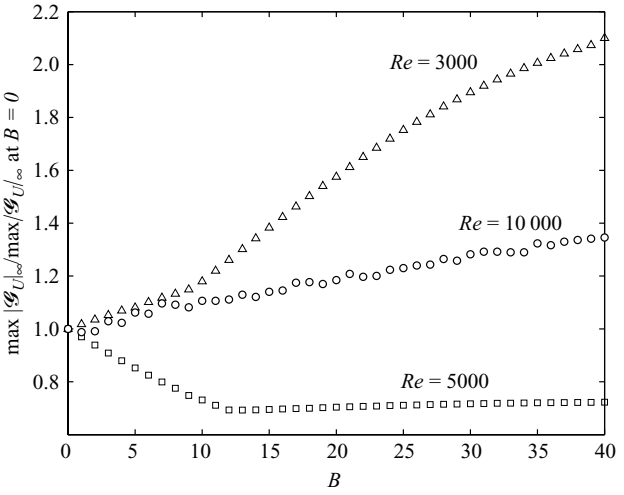

FIGURE 5. Evolution of the infinity norm of $\mathrm{Im}(\mathscr{G}_U)$ for the most sensitive modes as function of B at different values of Re, for $\alpha = 1$.

5. Minimal defects

We now set to analyse how small defects can alter the stability characteristics of the Bingham–Poiseuille flow and focus, in particular, on 'minimal defects' (Bottaro *et al.* 2003; Biau & Bottaro 2004; Gavarini, Bottaro & Nieuwstadt 2004; Ben Dov & Cohen 2007*a*,*b*), i.e. on the base flow deviations of minimal norm capable of yielding the largest amplification of instability modes. Small defects or deviations in the base velocity profile can arise because of geometrical imperfections in an experimental apparatus, or from fluctuations in the inflow conditions, or from the presence of roughness elements, gaps, junctions, etc., and can be responsible for the unexpected breakdown of the flow. Furthermore, it has been recently shown that minimal defects have a resemblance to *edge states* (Biau & Bottaro 2009), i.e. to those flow states which mediate the laminar–turbulent transition (Eckhardt *et al.* 2007). Whether this resemblance is just a coincidence or a matter of physical principles remains to be established.

5.1. *On the issue of regularization*

The velocity profile that we wish to slightly modify to assess the effect on the stability is $U_{ref} = 1 - y^2$; some constraint needs to be placed on the norm of the allowable variation, to prevent the solution from differing too much from the reference. In the disturbance energy equations the only term proportional to the Bingham number is negative definite (Nouar *et al.* 2007), i.e. it causes only dissipation of the perturbation energy; it can thus be anticipated that only base flow variations occurring in the low-viscosity near-wall region might have a significant destabilizing effect, while fluid layers near the plug zone (where DU approaches zero and $\mu \to \infty$) play mostly a passive role. This is suggested also by the fact that the sensitivity functions invariably tend to zero smoothly as the yield surface is approached. Furthermore, when modifying the base flow profile we need to ensure that DU does not change sign locally (cf. (2.5)), otherwise islands of unyielded material (with $\mu \to \infty$) would appear within the fluid domain. These requirements are dealt with by imposing that the allowable defect is of sufficiently small amplitude and confined to a zone *away* from the plug; this zone occupies more than 90 % of the whole yielded region. Thus, we constrain the velocity

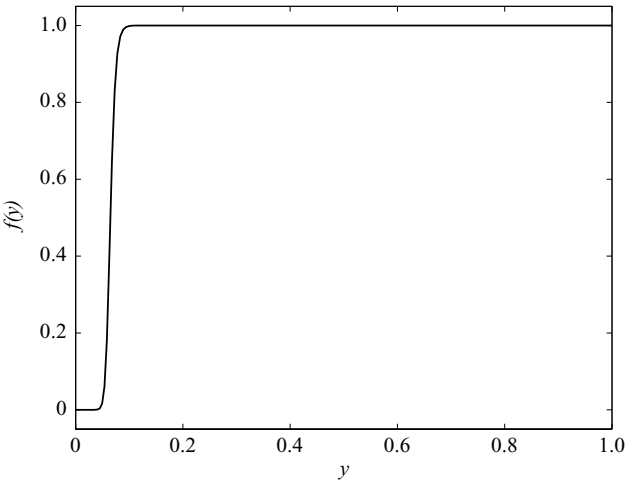

FIGURE 6. The filter function of (5.3).

variation to be of the form $f(y)\,\delta U$, so that (4.3) now reads

$$\delta\omega = (\mathscr{G}_U,\, f\delta U) = (f\mathscr{G}_U, \delta U), \tag{5.1}$$

and write a formal constraint on the allowable defect as

$$\int_0^1 [f(y)(U - U_{ref})]^2 \mathrm{d}y = \zeta\,; \tag{5.2}$$

$f(y)$ is a filter whose exact form is

$$f(y) = \left[1 + \tanh\left(\frac{(2y-1)+c_1}{c_2}\right)\right]^2; \tag{5.3}$$

by choosing $c_1 = 0.02$ and $c_2 = 0.9$ the filter is centred in $y = 0.054$ and has a support equal to approximately 0.08 units of length. It is displayed in figure 6. We have tested several other regularization functions and have observed that the final result is independent of the details of the filter, provided the support remains sufficiently narrow and $f(y) = 1$ to within 10^{-4} for $y > 0.1$. It is important to emphasize that the regularization procedure adopted has uniquely the scope of circumventing numerical difficulties associated with the vanishing value of DU as the yield surface is approached. Furthermore it is clear that through this regularization we exclude the possible breaking of the plug region and its replacement by an extensional region; the reader is referred to Balmforth & Craster (1999) for an asymptotic study of a thin-film Bingham-fluid flow characterized by extensional pseudoplug behaviour. The issue is worthy of future investigations.

5.2. *The gradient procedure*

To pursue the goal of finding a new base velocity profile $U(y)$ with the largest possible ω_i, under (5.2), we optimize the augmented functional $\mathscr{C}$ defined as

$$\mathscr{C} = \omega_i + \frac{\lambda}{2}\left\{\int_0^1 [f(y)(U - U_{ref})]^2 \mathrm{d}y - \zeta\right\}, \tag{5.4}$$

with λ a Lagrange multiplier. Setting the variation of $\mathscr{C}$ to zero, and using (5.1), it is found that

$$\left(\frac{\partial \mathscr{C}}{\partial U},\, \delta U\right) = 0, \tag{5.5}$$

with $\partial\mathscr{C}/\partial U$ the gradient of the functional, given by

$$\frac{\partial \mathscr{C}}{\partial U} = f(y)\{\,\mathrm{Im}[\mathscr{G}_U] + \lambda\, f(y)\,(U - U_{ref})\}, \tag{5.6}$$

and with the Lagrange multiplier equal to

$$\lambda = \pm\sqrt{\int_0^1 \frac{[\mathrm{Im}(\mathscr{G}_U)]^2}{\zeta}\,\mathrm{d}y}, \tag{5.7}$$

whenever $\partial\mathscr{C}/\partial U$ has been driven to zero. The negative root of λ is of interest in (5.7) above, since it leads to a maximization of the functional; conversely, in control problems it might be interesting to minimize ω_i, for example, stabilizing an otherwise unstable mode by acting on the shape of the base velocity profile (Hwang & Choi 2006).

A gradient algorithm is set up to proceed towards the maximum value of ω_i for each eigenmode, requiring the repeated evaluation of direct and adjoint eigenfunctions. Assuming that the velocity profile has been estimated at iteration (n), the successive step reads simply:

$$U^{(n+1)} = U^{(n)} - \phi\left[\frac{\partial \mathscr{C}}{\partial U}\right]^{(n)}, \tag{5.8}$$

with ϕ a positive relaxation parameter. This iterative procedure is extremely slow in attaining convergence since ϕ is kept very small to ensure that a given mode is always followed throughout its movement in the complex plain, i.e. to prevent the procedure from jumping from a mode to another (a common occurrence if care is not taken).

It is instructive to observe the difference between the results obtained in the presence and absence ($f(y) = 1\ \forall\ y$) of the filter. For this purpose we have drawn in figure 7 the base flow deviation that emerges after 40 000 gradient iterations under otherwise identical conditions. Neither of the two solutions has arrived at convergence yet, and in fact the profiles are not even (partially) superposed – despite being similar – because the presence of the filter affects the convergence rate of the iterative procedure. In the plot of ΔU near the yield surface the solution without filter displays numerical wiggles, which eventually pollute the whole field and lead to divergence of the procedure.

5.3. *Velocity and viscosity defects*

For very small values of ζ the minimal velocity defect is equal to the imaginary part of the sensitivity function. As the norm of the defect increases, the most disrupting defect can be very different from the sensitivity function of the most sensitive mode. This is highlighted in figure 8(a) where the velocity profiles U and U_{ref} as well as the minimal defects are displayed for a value of the defect norm $\zeta = 4 \times 10^{-5}$. In this figure, the least stable mode (numbered 1) has been targeted and followed iteratively. One can note that the defect is concentrated near the critical layer. The modified viscosity profile and the viscosity defect are shown in figure 8(b). It is worth observing that the viscosity gradient in correspondence to the critical layer and the wall has been rendered positive, which according to Govindarajan, L'vov & Procaccia (2001) is a destabilizing condition.

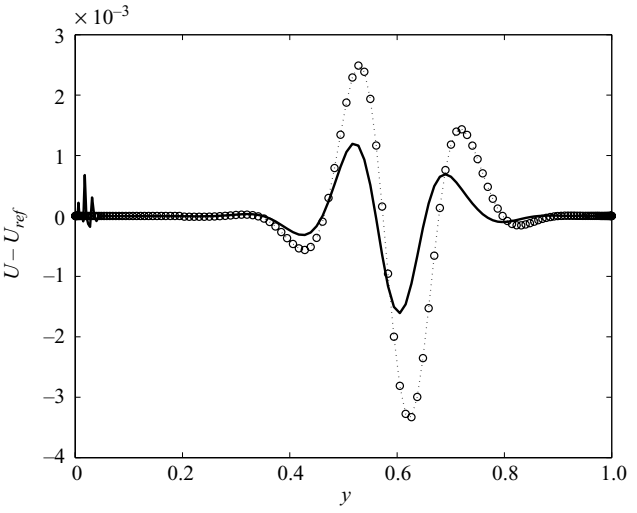

FIGURE 7. Comparison of $\Delta U = U - U_{ref}$ between the cases with (empty circles) and without (continuous line) filter in the gradient procedure. The results shown pertain to an intermediate step of the iterative procedure (5.8) for $\zeta = 10^{-6}$, with the relaxation factor ϕ fixed at the constant value of 5.2×10^{-4}. The mode which has been targeted is mode 13 of figure 3, i.e. the most sensitive one.

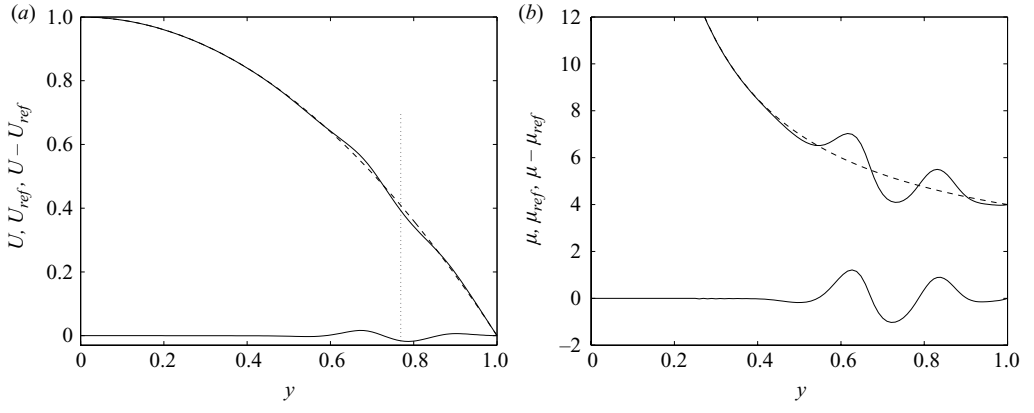

FIGURE 8. Velocity and viscosity defects at $Re = 2067$, $B = 6$, $\alpha = 1.73$ and $\zeta = 4 \times 10^{-5}$. (a) The dashed line represents the reference velocity profile $1 - y^2$. The continuous lines are the modified base flow and the velocity defect (lower curve). The vertical dotted line indicates the position of the critical layer. (b) The dashed line is the reference viscosity profile $1 + B/(2\,y)$. The continuous lines are the modified viscosity profiles and the viscosity defect (lower curve).

6. The ΔU-structured pseudospectrum

In §1 the qualitative difference between the ϵ-pseudospectrum and the ΔU-structured pseudospectrum has already been introduced. In more formal terms, the classical pseudospectrum of an operator L can be defined as

$$\Lambda_\epsilon(L) = \{\omega \in C \ : \ \omega \in \Lambda(L + \Delta) \text{ for some } \Delta \text{ with } \|\Delta\| \leqslant \epsilon\}, \tag{6.1}$$

with $\Lambda(L)$ the spectrum of L and Δ an unstructured disturbance operator. Other (equivalent) definitions exist but for comparison purpose the one given above is the

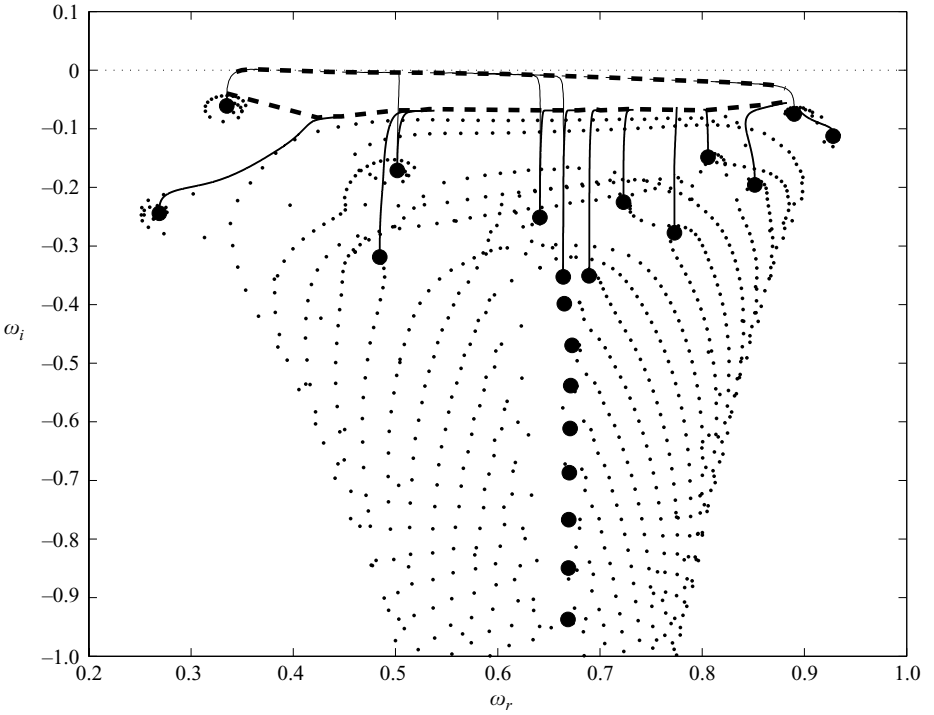

FIGURE 9. ΔU-structured pseudospectra for $\zeta = 10^{-5}$ (uppermost dashed curve) and $\zeta = 10^{-6}$ (lowermost dashed curve). See text for details.

most useful. The ΔU-structured pseudospectrum is

$$\Lambda_\zeta(L) = \{\omega \in C : \omega \in \Lambda[L(U_{ref} + \Delta U)] \text{ for some } \Delta U \text{ with } \|\Delta U\| \leqslant \zeta\}, \quad (6.2)$$

where the norm of ΔU is given by (5.2) and $\Delta U = U - U_{ref}$ represents a finite (typically small) distortion of the reference base flow. Since in hydrodynamic stability problems slight and practically unavoidable modifications in the base flow represent the primary source of differences between theory and experiments, it is argued that the pseudospectrum defined by (6.2) constitutes an alternative to the conventional ϵ-pseudospectrum which is based on a practically relevant norm.

The results shown in figure 9 are sufficient to illustrate our point. The bullets represent the spectrum for $Re = 5 \times 10^3$, $B = 2$ and $\alpha = 1$; the cloud of points around the unperturbed eigenmodes represent the ensemble of spectra computed by considering base flow defects of norm $\zeta = 10^{-6}$ of the form

$$\Delta U = \sqrt{\zeta\,[a/\pi]^{1/2}\,\mathrm{e}^{-a(y-y_0)^2}}, \quad (6.3)$$

with $a = 10\,000$ and y_0 spanning the y range from 0.1 to 0.9 in steps of 0.0125. Modes close to the crossing of branches experience the largest deviations from the reference positions; other modes (such as 1 and 8 in figure 3*a*) show smaller deviations. To draw the upper envelope of the ΔU-structured pseudospectrum we have successively targeted the first 13 modes and determined iteratively the worst possible base flow deformations. In the figure the 'trajectory' of each mode in the course of the iterations (5.8) is drawn with thin lines. The envelope of the converged, worst case scenario, i.e. the upper portion of the ΔU-pseudospectrum, is plotted with thick dashed lines

for the two cases of $\zeta = 10^{-6}$ and 10^{-5}. For the lower value of ζ the cloud of points is completely contained within the corresponding outer envelope and no unstable eigenvalues exist; for larger ζ the dashed line protrude into the unstable half-plane for a small range of frequencies around $\omega_r = 0.36$, revealing that disturbances can arise which are amplified exponentially in the presence of small defects in U. For yet larger values of ζ progressively larger unstable frequency bands are found.

It is possible to extend the contour of the ΔU-pseudospectra and trace the missing left and right quasi-vertical portions of the envelope, by searching for the base flow defect that maximizes (and minimizes) the *real* part of ω for each eigenmode. This task is however time consuming and not useful from the point of view of determining unstable modes for any given ζ, and thus we have not undertaken it.

The knowledge provided by the (portions of) structured pseudospectra displayed in figure 9 is not irrelevant: if an experimentalist can put an error bar on measurements of a steady base flow and can evaluate – even locally – the norm of the distortion from the idealized velocity profile, the ΔU-structured pseudospectrum can inform on whether an exponential instability of the flow should be excluded or not.

We wish to stress here that we are not trying to refute the importance of transient growth phenomena or of the ϵ-unstructured pseudospectra. We are simply arguing on the significance of a possible, well-identified cause of mismatch between the real flow and its idealization. Such a deviation can provoke exponential amplification of disturbances; on the other hand, the modified base flow is still highly non-normal (as shown, for example, by Bottaro *et al.* 2003) and is still susceptible to transient mechanisms. It is thus likely that exponential and transient effects are concurrently at play in the early stages of transition to turbulence, and neither should be discarded *a priori* (Biau & Bottaro 2004, 2009).

7. The neutral conditions

Knowing that instability can arise from the presence of base flow distortions, we have undergone a very comprehensive study to isolate critical conditions as function of the norm of the defect. The neutral solutions (Re_c, α_c) are displayed against B in figure 10 for different values of the norm of the base-flow deviation ζ. It is worth observing that, as opposed to the case of unstructured operator's perturbations for which the critical Reynolds number does not depend on B (Nouar *et al.* 2007), here, Re_c increases with B. For sufficiently, large B, the increase is close to the behaviour Re_c versus B derived by Frigaard & Nouar (2003) and Nouar *et al.* (2007) to define conditions of no energy growth at large B. We have also reported on the same figure (figure 10*a*) the two most popular phenomenological criteria (Hanks 1963 and Metzner & Reed 1955, the latter, originally proposed for pipe flows, has been generalized for any purely viscous fluid through ducts of arbitrary cross-section by Kozicki, Chou & Tiou 1966), proposed in the literature to predict the transition between the laminar and the turbulent regime (cf. also Nouar & Frigaard 2001). In terms of our parameters Re and B, they are given by

$$Re_c(Metzner\ and\ Reed) = 787.5\, B \frac{(1-y_0)^2}{y_0^3 - 3y_0 + 2}\,, \tag{7.1}$$

$$Re_c(Hanks) = 1050. \tag{7.2}$$

In reality, the literature contains about a dozen different phenomenological criteria. However, when the rheological properties of the fluid depart significantly from the

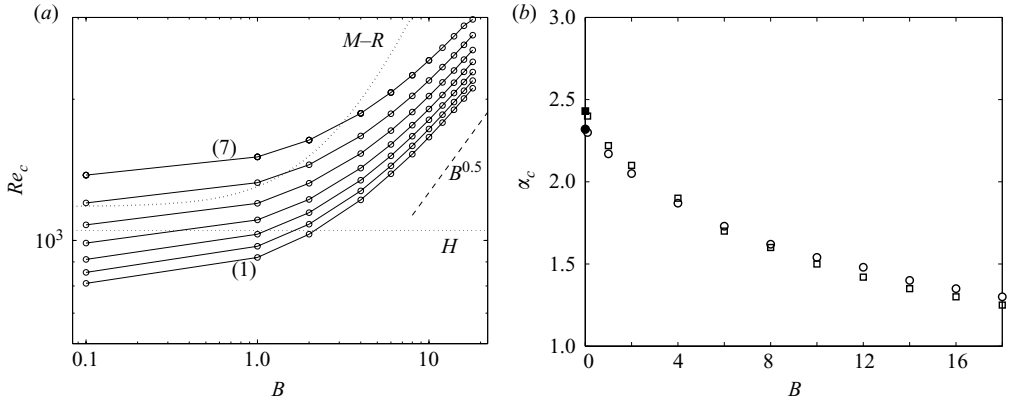

FIGURE 10. Variation of the critical conditions as function of the Bingham number for different values of ζ. (*a*) Critical Reynolds number: (1) $\zeta = 10^{-4}$, (2) $\zeta = 9 \times 10^{-5}$, (3) $\zeta = 8 \times 10^{-5}$, (4) $\zeta = 7 \times 10^{-5}$, (5) $\zeta = 6 \times 10^{-5}$, (6) $\zeta = 5 \times 10^{-5}$, (7) $\zeta = 4 \times 10^{-5}$. The dotted curves (H) and ($M - R$) correspond respectively to results reported by Hanks (1963) and Metzner & Reed (1955). The dashed curve represents the behaviour of the critical Reynolds number ensuring the no-energy growth condition for large B derived in Frigaard & Nouar (2003) and Nouar *et al.* (2007). (*b*) Critical wavenumber versus B for $\zeta = 10^{-4}$ (open square symbol) and $\zeta = 4 \times 10^{-5}$ (open circle symbol). The filled square and circle correspond to $B = 0$ (Newtonian Couette–Poiseuille flow) for $\zeta = 10^{-4}$ and $\zeta = 4 \times 10^{-5}$, respectively.

Newtonian case, the predictions provided by the phenomenological criteria diverge and there is no way to determine which criterion is preferable. The shortcoming of all criteria is that they do not contain information on the receptivity environment. It is however comforting to observe the similarity in behaviour between our curves (labelled (1) through (7) in figure 10*a*) with the phenomenological curve labelled $M - R$. It can be speculated that the transition data of Metzner & Reed (1955) correspond to a single inflow disturbance environment, and that – had the inflow condition been varied – the threshold curve would have been shifted vertically, resembling the curves of the present analysis. For sufficiently large values of B it is found that $Re_c \sim B^{0.5}$, like the theoretical result by Nouar *et al.* (2007). This behaviour lies in between the prediction of the phenomenological criteria proposed by Metzner & Reed (1955) and Hanks (1963). Also, the critical wavenumber behaves closely as $\alpha \sim B^{-0.5}$. Finally, for a reasonably large range of flow defect norms, the critical wavenumber has found to be essentially independent of ζ.

The critical conditions as function of the Bingham number in terms of parameters which are not normalized with the width of the yielded zone, i.e. parameters without $\tilde{}$ (cf. § 3.3), are represented in figure 11. In the same figure (figure11*a*) we have also reported experimental points from Hanks & Pratt (1967); they follow rather closely our family of curves over the B range considered.

The variation of the critical Reynolds number with the norm of the base flow deviation ζ is displayed in figure 12(*a*) for different values of B. The data points in this figure may be described by a relation of the kind $Re_c \sim 1/\zeta^{\gamma}$. In figure 12(*b*) we have drawn the variation of γ with the Bingham number; it decreases with increasing B, remaining in the vicinity of 0.5 which is the value obtained for some shear flows in the Newtonian case (Bottaro *et al.* 2003; Gavarini *et al.* 2004). These results indicate that the size of the perturbation necessary to initiate transition in this nominally subcritical flow decreases (proportionally) more sharply with Re for large B, and this

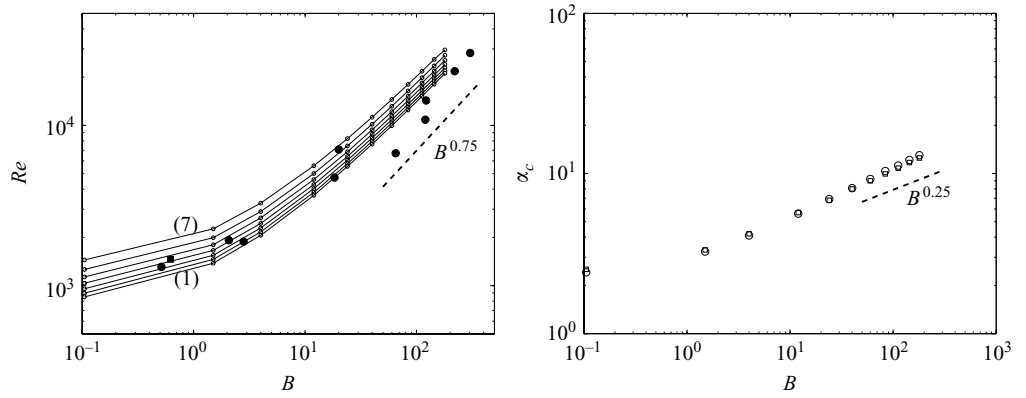

FIGURE 11. Variation of the unscaled critical conditions as function of the unscaled Bingham number for different values of ζ. (*a*) Critical (unscaled) Reynolds number for the same ζ values as in figure 11. The dashed curve represents the behaviour of the critical Reynolds number ensuring the no-energy growth condition for large B derived in Frigaard & Nouar (2003) and Nouar *et al.* (2007). The filled circles are experimental critical points obtained by Hanks & Pratt (1967). (*b*) Critical (unscaled) wavenumber versus B for $\zeta = 10^{-4}$ (open square symbol) and $\zeta = 4 \times 10^{-5}$ (open circle symbol). The dashed curve represents the behaviour of the critical wavenumber ensuring the no-energy growth condition for large B.

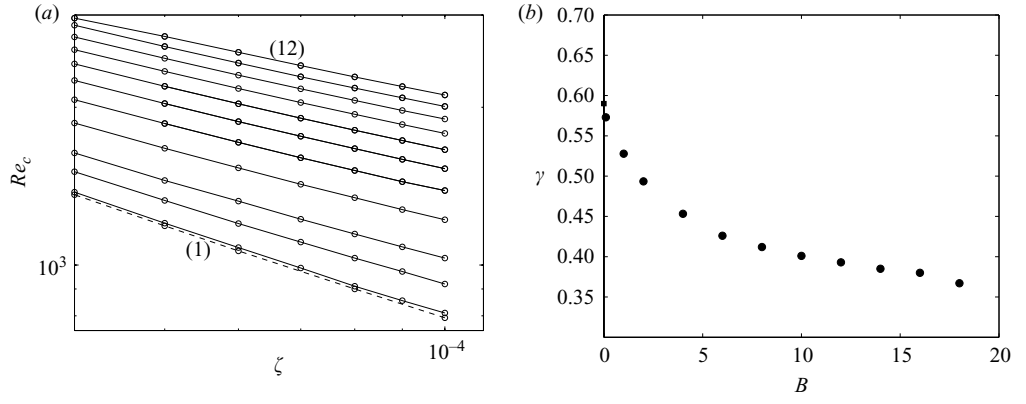

FIGURE 12. (*a*) Variation of the critical Reynolds number as function of the norm of the base-flow deviation: (1) Dashed line corresponds to $B = 0$, i.e. Couette-Poiseuille flow of Newtonian fluid, (2) $B = 0.1$, (3) $B = 1$, (4) $B = 2$, (5) $B = 4$, (6) $B = 6$, (7) $B = 8$, (8) $B = 10$, (9) $B = 12$, (10) $B = 14$, (11) $B = 16$, (12) $B = 18$. In this figure variables are scaled with the thickness of the yielded region. (*b*) Exponent γ versus B. The square symbol corresponds to the Newtonian case ($B = 0$).

is a consequence of the shear thinning behaviour of the fluid. In terms of unscaled variables (i.e. when the reference length is the channel half-thickness) the same values of the exponent γ are recovered, an indication that γ expresses well the effect of shear thinning.

8. Concluding remarks

The flow of a Bingham fluid in a channel is asymptotically stable to infinitesimal disturbances, a fact which renders challenging and interesting the investigation of

transitional paths. The linear transient growth approach has been pursued for the present flow configuration by Nouar *et al.* (2007), but the usefulness of optimal disturbances has been disputed recently by Biau & Bottaro (2009) who argue on the crucial importance of nonlinear terms to sustain a distorted flow in the channel. A different route of transition can be envisioned starting from the realization that the base flow around which linearization is performed is just an idealization, whereas in reality small defects inevitably occur. This alternative approach is also based on linear stability equations (although the base flow distortion is of finite amplitude) and admits exponentially growing modes as solutions. It has been proposed by Bottaro *et al.* (2003), and has shown some success in capturing features of transition in pipe flow (Gavarini *et al.* 2004; Ben Dov & Cohen 2007*a*,*b*). It is here applied for the first time to the motion of a non-Newtonian fluid, with the goal of identifying scaling laws of the critical Reynolds number as function of the yield stress (expressed through the Bingham number) and the disturbance environment (measured by the norm of the deviation of the actual base flow from its idealized counterpart).

The procedure starts with the definition of a function quantifying the sensitivity of an eigenvalue (of the linear stability operator) to variations in the base flow (hence in the operator itself). Results show that such a function varies little with the characteristic spanwise dimension of the disturbance mode, and this is used as an argument to focus attention on a single-spanwise-wavenumber disturbance ($\beta = 0$). As already found in the Newtonian case, the most sensitive modes are those at the intersection of the branches of the spectrum; minimal defects (computed from the sensitivity function after setting up a proper variational problem) display peaks in the proximity of the critical layer, rendering the flow inviscidly unstable. The deformations in the viscosity profiles have trends similar to the corresponding base flow deviations.

Neutral conditions have then been identified as function of the disturbance environment (modelled by the value of ζ); this is a lengthy procedure which requires repeated searches in a multidimensional parameter space. The most significant result is that the critical Reynolds number increases with the Bingham number (which expresses the degree of nonlinearity of the effective viscosity at the wall when tilde variables are employed), in agreement with asymptotic laws by Frigaard & Nouar (2003) and Nouar *et al.* (2007), and with experimental neutral points by Hanks & Pratt (1967). Larger values of Re_c are found for cleaner inflow environments, as one would intuitively expect. On the other hand, the wavelength of the neutral disturbance mode does not vary with the disturbance level, with shorter waves (cf. figure 11*b*) preferentially excited with the increase of the Bingham number.

As to one of the stated goals of the present investigation, i.e. scaling laws of transition, it has been found that $Re_c \sim \zeta^{-\gamma}$, with γ a decreasing function of the yield stress parameter B. Similar scaling laws have been obtained recently by various linear and nonlinear theoretical means, as well as through experiments, but only for the flow of Newtonian fluids. For example, experiments by Peixinho & Mullin (2006) in a pipe have found a scaling with $\gamma = 0.5$, recovered theoretically by Gavarini *et al.* (2004), Ben Dov & Cohen (2007*a*) and Ben Dov & Cohen (2007*b*). For the same flow case, Trefethen *et al.* (2000) have assembled a number of experimental, theoretical and numerical studies, based on which it is $0.27777 \leqslant \gamma \leqslant 0.41666$. For plane Poiseuille flow, using asymptotic analysis, Chapman (2002) has found $\gamma = 0.3333$ when transition is initiated by streamwise-homogeneous initial perturbations (confirmed experimentally by Philip, Svizher & Cohen 2007) and $\gamma = 0.4$ for oblique initial disturbances. For both classes of initial perturbation, Chapman (2002) has also found

that $\gamma = 0.5$ for the Couette flow, a value also recovered in the numerical simulations by Kreiss, Lundbladh & Henningson (1994). The scaling exponent found in the present contribution is close to all of these values and changes smoothly from 0.57 (when $B = 0$) to 0.37 (when $B = 18$). Having established the dependence of Re_c with ζ we have the answer to one important question: if an experimentalist can estimate the norm of the expected deviation from ideal conditions, the threshold curves obtained (corresponding to worst case scenario) indicate whether an instability can be ruled out.

This work puts just a brick to a more comprehensive building. Many effects have been ignored, starting from the fact that the stability operator is non-normal and, as a consequence, transient amplification is concurrently at play with exponential growth in causing breakdown. Another fact is that nonlinearities must play a role in the breakdown of the flow, and recent developments, in the Newtonian frame, concern the existence of unstable nonlinear solutions and edge states (Eckhardt *et al.* 2007), which provide the skeleton around which transitional and turbulent trajectories are organized in phase space. A somewhat loose relation between edge state and minimal defects has been found for a specific configuration (Biau & Bottaro 2009), but more work is in order to connect these concepts, a challenging undertaking particularly when working in the non-Newtonian realm.

Appendix. Expressions of $\mathscr{I}_1$, $\mathscr{I}_2$ and $\mathscr{I}_3$

The terms $\mathscr{I}_1$, $\mathscr{I}_2$ and $\mathscr{I}_3$ of (4.4) are

$$\mathscr{I}_1 = \alpha\, k^2\, bw - \alpha\beta\, wDa + \mathrm{i}\alpha[\alpha^2\, a\, v + vD^2a + 2Da\, Dv] - \mathrm{i}\alpha\,\beta\,[2\,bDv + vDb], \quad \text{(A 1)}$$

$$\begin{aligned}\mathscr{I}_2 = {} & \alpha^2\,\beta^2 D\left[\frac{a\,v}{\Gamma^2}\right] + (4\alpha^2 + \beta^2)D\left[\frac{Da\,Dv}{\Gamma^2}\right] \\ & - \beta\,(k^2 + \alpha^2)D\left[\frac{b\,Dv}{\Gamma^2}\right] - \alpha^2\, D\left[\frac{D(bv)}{\Gamma^2}\right] \\ & + \mathrm{i}\,\beta\,k^2\, D\left[\frac{D\,(a\,w)}{\Gamma^2}\right] - (k^2 + \alpha^2)\, D\left[\frac{a\,Dw}{\Gamma^2}\right] \\ & - \mathrm{i}\alpha^2\, D\left[\frac{D(b\,Dw)}{\Gamma^2}\right], \end{aligned} \quad \text{(A 2)}$$

$$\mathscr{I}_3 = -\mathrm{i}\,a(D^2\, v - \alpha^2\, v) + \beta\, a\, Dw - \mathrm{i}\beta\, b\, Dv + k^2\, b\, w. \quad \text{(A 3)}$$

REFERENCES

Abbas, M. A. & Crowe, C. T. 1987 Experimental study of the flow properties of homogeneous slurry near transitional Reynolds numbers. *Intl J. Multiph. Flow* **13**, 387–364.

Balas, G. J., Doyle, J. C., Glover, K., Packard, A. & Smith, R. 2001 *μ-Analysis and Synthesis Toolbox. User's Guide*. Version 4. The Mathworks.

Balmforth, N. J. & Craster, R. V. 1999 A consistent thin-layer theory for Bingham plastics *J. Non-Newton. Fluid Mech.* **814**, 65–81.

Barnes, H. A. 1999 The yield stress: a review or '$\pi\alpha\nu\tau\alpha\ \rho\epsilon\iota$': everything flows? *J. Non-Newton. Fluid Mech.* **81**, 133–178.

Ben Dov, G. & Cohen, J. 2007*a* Critical Reynolds number for a natural transition to turbulence in pipe flows. *Phys. Rev. Lett.* **98**, 064503.

Ben Dov, G. & Cohen, J. 2007*b* Instability of optimal non-axisymmetric base-flow deviations in pipe Poiseuille flow. *J. Fluid Mech.* **588**, 189–215.

Bercovier, M. & Engelman, M. 1980 A finite-element method for incompressible non-Newtonian flows *J. Comput. Phys.* **36**, 313–326.

Bergström, L. B. 2005 Nonmodal growth of three-dimensional disturbances on plane Couette–Poiseuille flows. *Phys. Fluids* **17**, 014105.1–014105.10

Beverly, C. R. & Tanner, R. I. 1992 Numerical analysis of three-dimensional Bingham plastic flow. *J. Non-Newton. Fluid Mech.* **42**, 85–115.

Biau, D. & Bottaro, A. 2004 Transient growth and minimal defects: two possible initial paths of transition to turbulence in plane shear flows. *Phys. Fluids* **16**, 3515–3529.

Biau, D. & Bottaro, A. 2009 An optimal path to transition in a duct. *Phil. Trans. R. Soc,* A **367**, 529–544.

Biau, D., Soueid, H. & Bottaro, A. 2008 Transition to turbulence in duct flow. *J. Fluid Mech.* **596**, 133–142.

Bird, R. B., Dai, G. C. & Yarusso, B. J. 1983 The rheology and flow of viscoplastic materials. *Rev. Chem. Engng* **1**, 1–70.

Bottaro, A., Corbett, P. & Luchini, P. 2003 The effect of base flow variation on flow stability. *J. Fluid Mech.* **476**, 293–302.

Chapman, S. J. 2002 Subcritical transition in channel flows. *J. Fluid Mech.* **451**, 35–97.

Coussot, P. 1999 Saffman–Taylor instability in yield-stress fluids. *J. Fluid Mech.* **380**, 363–376.

De Kee, D. & Chan Man Fong, C. F. 1993 A true yield stress? *J. Rheol.* **37**, 775–776.

Dodge, D. W. & Metzner, A. B. 1959 Turbulent Flow of Non-Newtonian Systems. *A.I.Ch.E J.* **5**, 189–204.

Eckhardt, B., Schneider, T. M., Hof, B. & Westerweel, J. 2007 Turbulence transition in pipe flow *Annu. Rev. Fluid Mech.* **39**, 447–468.

Escudier, M. P., Poole, R. J., Presti, F., Dales, C., Nouar, C., Graham, L. & Pullum, L. 2005 Observations of asymmetrical flow behaviour in transitional pipe flow of yield-stress and other shear thinning liquids. *J. Non-Newton. Fluid Mech.* **127**, 143–155.

Escudier, M. P. & Presti, F. 1996 Pipe flow of thixotropic liquid. *J. Non-Newton. Fluid Mech.* **62**, 291–306.

Esmael, A. & Nouar, C. 2008 Transitional flow of a yield-stress fluid in a pipe: evidence of a robust coherent structure. *Phys. Rev.* E **77**, 057302.

Frigaard, I. A., Howison, S. D. & Sobey, I. J. 1994 On the stability of Poiseuille flow of a Bingham fluid. *J. Fluid Mech.* **263**, 133–150.

Frigaard, I. A. & Nouar, C. 2003 On three-dimensional linear stability of Poiseuille flow of Bingham fluids. *Phys. Fluids* **15**, 2843–2851.

Frigaard, I. A. & Nouar, C. 2005 On the usage of viscosity regularisation methods for visco-plastic fluid flow computation. *J. Non-Newton. Fluid Mech.* **127**, 1–26.

Gavarini, I., Bottaro, A. & Nieuwstadt, F. T. M. 2004 The initial stage of transition in cylindrical pipe flow: role of optimal base-flow distortions. *J. Fluid Mech.* **517**, 131–165.

Georgievskii, D. V. 1993 Stability of two and three-dimensional viscoplastic flows, and generalized Squire theorem. *Isv. Akad. Nauk SSR Mekh. Tverd. Tela* **28**, 117–123.

Govindarajan, R., L'vov, V. S. & Procaccia, I. 2001 Retardation of the onset of turbulence by minor viscosity contrast. *Phys. Rev. Lett.* **87**, 174501.1–174501.4.

Gupta, G. K. 1999 Hydrodynamic stability analysis of the plane Poiseuille flow of an electrorheological fluid. *Intl J. Nonlinear Mech.* **34**, 589–602.

Guzel, B., Burghelea, T., Frigaard, I. & Martinez, M. 2009*b* Observation of laminar-turbulent transition of a yield stress fluid in Hagen–Poiseuille flow. *J. Fluid Mech.* **627**, 97–128.

Guzel, B., Frigaard, I. & Martinez, M. 2009*a* Predicting laminar-turbulent transition in Poiseuille pipe flow for non-Newtonian fluids. *Chem. Engng Sci.* **64**, 254–264.

Hanks, R. W. 1963 The laminar turbulent transition for fluids with a yield stress. *A.I.Ch.E. J.* **9**, 306–309.

Hanks, R. W. & Christiansen, E. B. 1962 The laminar-turbulent transition in nonisothermal flow of pseudoplastic fluids in tubes. *A.I.ChE. J.* **8**, 467–471.

Hanks, R. W. & Pratt, D. R. 1967 On the flow of Bingham plastic slurries in pipes and between parallel plates. *Soc. Pet. Eng. J.* **87** (4), 342–346.

Hedström, B. O. A. 1952 Flow of plastic materials in pipes. *Ind. Engng Chem.* **44**, 652–656.

Hwang, Y. & Choi, H. 2006 Control of absolute instability by basic flow modification in a parallel wake at low Reynolds number. *J. Fluid Mech.* **87** (4), 342–346.

Kreiss, G., Lundbladh, A. & Henningson, D. S. 1994 Bounds for threshold amplitudes in subcritical shear flows. *J. Fluid Mech.* **270**, 175–198.

Kozicki, W., Chou, C. & Tiou, C. 1966 Non-Newtonian flow in ducts of arbirary cross-sectional shape. *Chem. Engng Sci.* **21**, 665–679.

Lips, G. C. & Denn, M. M. 1984 Flow of Bingham fluids in complex geometries. *J. Non-Newton. Fluid Mech.* **14**, 337–346.

Mack, L. M. 1976 A numerical study of the temporal eigenvalue spectrum of the Blasius boundary layer. *J. Fluid Mech.* **73**, 497–520.

Metzner, A. B. & Park, M. G. 1964 Turbulent flow characteristics of viscoelastic fluids. *J. Fluid Mech.* **20** 291–303.

Metzner, A. B. & Reed, J. C. 1955 Flow of non-Newtonian fluids – Correlation of the laminar, transition and turbulent flow regions. *A.I.ChE. J.* **1**, 434–440.

Meyer, W. A. 1966 A correlation of the frictional characteristics for turbulent flow of dilute viscoelastic non-Newtonian fluids in pipes. *A.I.ChE. J.* **12**, 522–525.

Mishra, P. & Tripathi, G. 1971 Transition from laminar to turbulent flow of purely viscous non-Newtonian fluids in tubes. *Chem. Engng Sci.* **26**, 915–921.

Nguyen, Q. D. & Boger, D. V. 1992 Measuring the flow properties of yield stress fluids. *Annu. Rev. Fluid Mech.* **24**, 47–88.

Nouar, C. & Frigaard, I. 2001 Nonlinear stability of Poiseuille flow of a Bingham fluid: theoretical results and comparison with phenomenological criteria. *J. Non-Newton. Fluid Mech.* **100**, 127–149.

Nouar, C., Kabouya, N., Dusek, J. & Mamou, M. 2007 Modal and non-modal linear stability of the plane-Bingham–Poiseuille flow. *J. Fluid Mech.* **577**, 211–239.

Papanastasiou, T. C. 1987 Flows of materials with yield. *J. Rheol.* **31**, 385–404.

Park, J. T., Mannheimer, R. J., Grimley, T. A. & Morrow, T. B. 1989 Pipe flow measurements of a transparent non-Newtonian Slurry. *ASME J. Fluids Engng* **111**, 331–336.

Peixinho, J. & Mullin, T. 2006 Decay of turbulence in pipe flow. *Phys. Rev. Lett.* **96**, 094501.

Peixinho, J., Nouar, C., Desaubry, C. & Théron, B. 2005 Laminar transitional and turbulent flow of yield stress fluid in a pipe. *J. Non-Newton. Fluid Mech.* **128**, 172–184.

Philip, J., Svizher, A. & Cohen, J. 2007 Scaling law for a subcritical transition in plane Poiseuille flow. *Phys. Rev. Lett.* **98**, 154502.

Potter, M. C. 1966 Stability of plane Couette–Poiseuille flow. *J. Fluid Mech.* **24**, 609–619.

Ryan, N. W. & Johnson, M. M. 1959 Transition from laminar to turbulent flow in pipes. *A.I.Ch.E. J.* **5**, 433–435.

Shaver, R. G. & Merill, E. W. 1959 Turbulent flow of pseudoplastic polymer solutions in straight cylindrical tubes. *A.I.Ch.E. J.* **5**, 181–188.

Slatter, P. T. 1999 The laminar turbulent transition prediction for non-Newtonian Slurries. In *Proceedings of the International Conference problems in Fluid Mechanics and Hydrology,* Prague, Czech Republic, 247–256.

Trefethen, L. N., Chapman, S. J., Henningson, D. S., Meseguer, A., Mullin, T. & Nieuwstadt, F. T. M. 2000 Threshold amplitudes for transition to turbulence in a pipe. *Numerical Analysis Report 00/17,* Oxford University Computing Laboratory.

Trefethen, L. N., Trefethen, A. E., Reddy, S. C. & Driscoll, T. A. 1993 Hydrodynamic stability without eigenvalues. *Sciences* **261**, 578–584.